The Early Evening Surface-Layer Transition: Temporal and Spatial Variability

OTÁVIO C. ACEVEDO AND DAVID R. FITZJARRALD

Atmospheric Sciences Research Center, The University at Albany, State University of New York, Albany, New York

(Manuscript received 5 July 2000, in final form 31 January 2001)

ABSTRACT

On clear nights with appreciable radiative cooling, rates of change of mean quantities observed in the first 1 or 2 h after sunset are many times larger than they are subsequently until sunrise. These variations include large temperature drops, specific humidity increases, and abrupt wind speed decay. The early evening transition (EET) is dominated by vertical surface flux convergence as the turbulent mixing layer becomes confined to a shallow stable layer near the surface. Effects of surface heterogeneities are enhanced by the subsequent small eddy size, so that spatial variability of mean variables peaks during the EET. Hilltops do not experience such large variations at EET, as turbulence persists longer at those locations. Wind speed decays faster at obstructed sites, which show earlier transitions. The Richardson number increases exponentially at the EET, and the rate of exponential increase is proportional to the rate of wind decay. Qualitative aspects of the EET at a single point are resolved by a two-layer model, similar to those currently used in parameterizations of the surface exchange in mesoscale simulations. However, in order to simulate the different behaviors observed in an area as big as one grid cell in a mesoscale model, very different values of the geostrophic wind need to be imposed. A large eddy model is used to verify that the specific humidity jump and maximum cooling rate during the EET are primarily the consequence of enhanced vertical flux divergence, though in later stages of the EET, advective effects become more important.

1. Introduction

Under clear skies, surface state variables (temperature, specific humidity q, and the mean wind) often exhibit larger variations in the first 1 or 2 h following sunset than during the rest of the night. This period of enhanced changes at the surface is the early evening transition (EET) and results from the decay of turbulent activity. Nieuwstadt and Brost (1986) studied turbulence decay, restraining the analysis to the residual layer that remains above the newly formed stable layer (SL) at the surface. They found that in this region, turbulent kinetic energy (TKE) scales to dimensionless time $\tau = tw_*/h$ (w_* and h refer to the standard convective boundary layer scales, just before the beginning of the surface cooling), essentially the same prediction obtained from simple dimensional analysis (Tennekes and Lumley 1972). TKE remains approximately constant until $\tau \approx 1$, decreasing strongly (as $1/\tau$) after this time. The timescale for TKE decay in the residual layer is on the order of tens of minutes. Sorbjan (1997) used more realistic boundary conditions, but found similar results. These studies did not focus on the turbulence decay at the surface, which has important consequences on the state variables. This is a more complex problem, since the presence of the surface favors shear production of turbulence, which in the EET competes with the TKE removal via the incipient stable stratification. TKE decay at the surface can go on for some hours, a time much longer than typical surface-layer characteristic timescale ($\kappa z/u_* \approx 2$ min, where κ is the von Kármán constant and u_* is the friction velocity).

As TKE decays, mixing activity near the surface is confined to a much shallower layer than previously. The boundary layer thickness does not drop, but rather a new stable surface-layer develops. Accompanying the decay in mixing is a rise in the near-surface specific humidity (q), which has been noted for some time. Geiger (1971, p. 105) noted that the ''well-known double wave in specific humidity'' was apparent in data obtained in Britain in the early 1950s. Earlier, W. D. Flower's more comprehensive 1932 observations at Ismailia Egypt (Flower 1937) showed the early evening q maximum to accompany rapidly dropping surface temperature and decaying wind speed (Fig. 1a). Flower found that the time of zero temperature gradient (1.1–16.2 m layer) led sunset on average by 51 min on clear evenings.

Fitzjarrald and Lala (1989, hereafter FL89) showed that the broad maximum evident in the classic studies of hourly averages is really a rapid ''jump.'' They associated the q jump with the evaporation that decaying surface layer turbulence promotes. They noted that the

Corresponding author address: Otávio C. Acevedo, 251 Fuller Road, Albany, NY, 12203.
E-mail: oacevedo@asrc.cestm.albany.edu

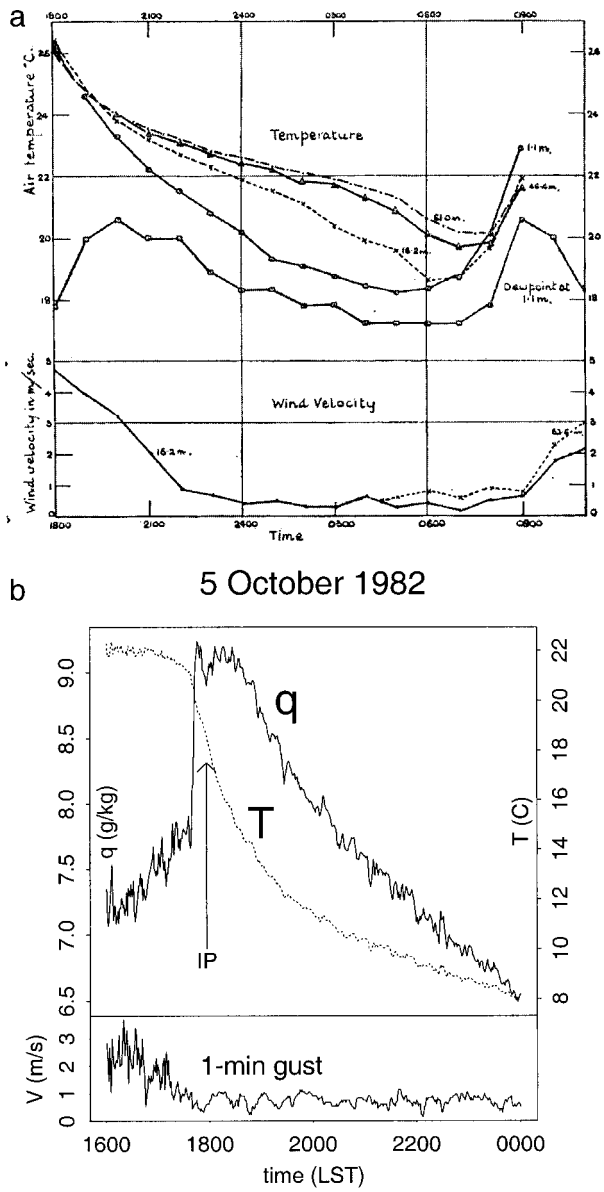

FIG. 1. (a) Behavior of the temperature (1.1, 16.2, and 46.4 m), dewpoint (1.1 m), and wind velocity (16.2 m) on occasions when fog developed in Oct 1932 at Ismailia, Egypt. Time axis is labeled from 1800 to 0900 LST [detail from Flower (1937), Fig. 13, p. 41]. (b) (upper panel) Time evolution of 1-min-averaged specific humidity (solid) and temperature (dotted) in 5 Oct 1982 at station 18 (located near Albany, NY; see below). The inflection point in the temperature series is indicated by letters ''IP.'' (lower panel) The maximum wind gust in 1-min periods.

jump likely results from convergence of the rapidly dropping evaporation rate into the stable surface layer, though horizontal advection may play a role in some situations. A typical example (Fig. 1b) illustrates a jump of 1.5 g kg^{-1} in about 10 min, though q jumps that occur over as little as 6 min were observed. FL89 noted that during transition, the temperature often shows a temporal inflection point (denoted by ''IP'' in Fig. 1b), approximated by

$$z_s \frac{\partial^2 T}{\partial t^2} \approx \frac{\partial(\overline{w\theta})_0}{\partial t} + \frac{\partial R_{n0}}{\partial t}, \tag{1}$$

where z_s is a height at which both the sensible heat flux and net radiation can be neglected, T is surface layer temperature, $(\overline{w\theta})_0$ is the surface sensible heat flux, and R_{n0} is net radiative flux at the surface. At the end of the afternoon both terms in the rhs of (1) are negative, as both the sensible heat flux and net radiation decrease from positive to negative values. Temperature drops abruptly at this time, with R_{n0} and $(\overline{w\theta})_0$ reaching a minimum, also observed by Caughey et al. (1979). As turbulence dies, the absolute value of $(\overline{w\theta})_0$ decreases and the first term on the rhs becomes positive. The rate of temperature decrease reaches a maximum (inflection point) when the sum $[(\overline{w\theta})_0 + R_{n0}]$ is a minimum. After that, the lhs is positive, resulting in a smaller rate of temperature decrease.

The importance of the EET is illustrated by a case shown in Fig. 1. The sharp moisture increase that happens over 10 min just before 1800 LST is as large as the total variation in the subsequent 4 h. In the same 10-min period the temperature decreases an amount equivalent to that which occurs during more than 2 h of cooling later at night.

Practical consequences of this transition include:

1) *Fog formation*, studied by Fitzjarrald and Lala (1989). The q jump is often large enough to cause saturation at the surface and largely determines the time when fog will occur.
2) *Small-scale frost forecast.* The EET temperature variability may determine whether the surface will cool below freezing.
3) *Air quality issues.* The transition seen in moisture is also expected to happen for other scalars with surface fluxes and may determine whether or not exceedance limits for these quantities are reached.

EET processes have been studied since the first decades of this century. Taylor (1917) looked at anemograms and thermograms on different nights, and noted that strong nocturnal cooling occurred only in the cases of weak, nonturbulent winds. He suggested that turbulent decay at night would not occur if a cloud deck kept the surface relatively warm. Richardson (1920) addressed the same problem from the TKE budget point-of-view. His comparison of shear production and buoyant destruction of turbulence in the early evening led to the definition of the Richardson number.

Relatively few field studies specifically focused on EET. Grant (1997) presented the most complete recent study, and it used only three nights of measurements. He studied the dynamical variables causing and controlling EET processes, with emphasis on describing the turbulent fluxes. These measurements show the presence of strongly vertically curved profiles of sensible heat

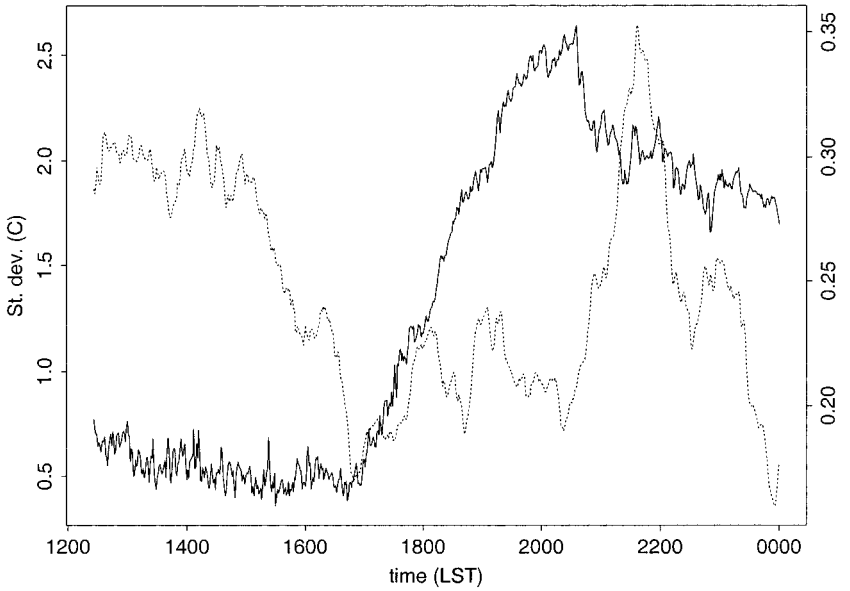

FIG. 2. Solid line: spatial standard deviation of temperature, calculated at each minute from 26 station values (scale on left axis). Dotted line: mean temporal standard deviation. It is calculated at each station, for 30-min periods, after trend removal. Average results for the 26 stations are presented (scale on right axis).

and momentum fluxes that are initially restricted to a 400-m-thick layer, adjacent to the surface. Caughey et al. (1979) found similar features in data from the Minnesota experiment. Mahrt et al. (1999) analyzed the results of aircraft measurements during EET, and pointed to a gentle q increase at EET. They also studied the morning transition, observing many local surface heat flux maxima early in the morning. By noontime a broad, spatially spread maximum occurs, indicating that the spatial scale of horizontal variability in the boundary layer is inversely proportional to the turbulent intensity. Mahrt (1981) observed the increase in momentum flux divergence at EET despite the decrease in turbulent intensity and showed that this phenomenon contributes to the formation of nocturnal low-level jets. Lenschow et al. (1979) identified a rapid transition in the morning, much more common in valley locations than on plateaus. More recently, the CASES-99 project (LeMone et al. 2000) has as one of its main objectives the understanding of the early evening and morning transition periods.

During the few hours of the EET, large horizontal gradients of temperature, moisture, wind speed, and direction develop and can persist over the rest of the night. Processes are controlled locally, as turbulent levels and eddy sizes are small, enhancing the importance of local site characteristics. This aspect is shown by the comparison of the temporal ($\sigma_{T,\text{temp}}$) and spatial ($\sigma_{T,\text{spat}}$) standard deviations of temperature for a region (Fig. 2). In the middle of the day, large eddies produce larger fluctuations of temperature at any one place (large $\sigma_{T,\text{temp}}$), but these move with the ambient wind, promoting statistical spatial homogeneity (small $\sigma_{T,\text{spat}}$). Turbulent activity decreases until $\sigma_{T,\text{temp}}$ reaches a minimum at the beginning of the EET, when surface layer flux divergence is dominant. At this point mixing is a much more local process and leads to a rapid increase of $\sigma_{T,\text{spat}}$. After some hours, turbulence has decayed almost completely in the whole network, so that $\sigma_{T,\text{spat}}$ reaches a peak at the end of the EET. On the bulk of calm nights, limited turbulent activity prevents subsequent large changes in the variables, so that enhancement of horizontal gradients can only occur in the case of significant spatial variations of radiative forcing. These can be induced by the presence of buildings (Sproken-Smith and Oke 1999) or by localized clouds. We do not address these effects here.

The enhancement of spatial heterogeneity at EET poses difficulties for assessing the representativeness of surface observations and the subsequent modeling of exchanges at this time of the day. McNider et al. (1995) showed that currently used parameterizations of surface exchanges in mesoscale models are strongly dependent on the initial conditions. Very different results are obtained by these models, depending upon whether there is coupling between the surface and upper boundary layer. Derbyshire (1999) argued that ''apparently some property of the SBL, or of its parameterization, allows or prevents 'decoupling' in a manner not yet fully understood.'' The way these models handle turbulence decay and subsequent response of the other variables at EET, therefore, strongly determines what they predict for the remainder of the night.

Previous observational studies described the evolu-

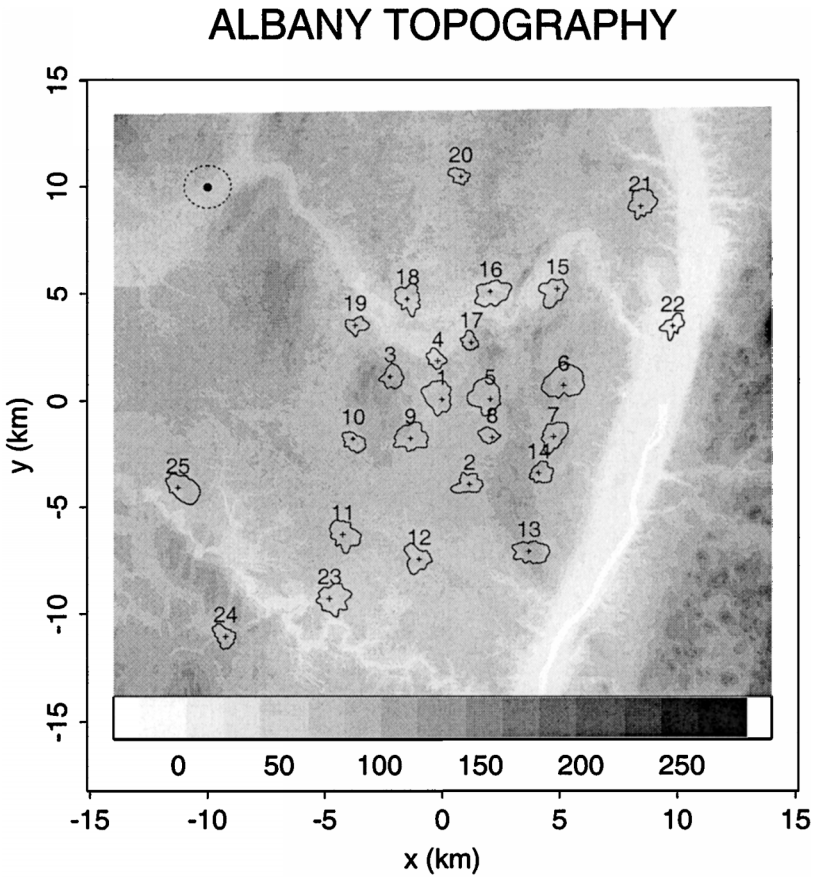

FIG. 3. Location of the stations and topography of the Albany region, with the grayscale in meters. Hudson (N–S orientation), Mohawk (E–W, near stations 15–19), and Normanskill (E–W, near stations 23–25) rivers are visible. At each station, the transmission factor for each direction is shown. Perfect transmission is given by the circle at upper left.

tion of flux divergence during EET, but they did not focus on the implications of this evolution in mean variables and the control they exert on the nocturnal surface layer. In this work we demonstrate the importance of EET in the control of temperature, specific humidity, wind magnitude, and their spatial distributions. We do this observationally, using data collected by a network of 26 surface stations that operated for 2 months during the fall of 1982 in the region of Albany, New York, and numerically, with a large eddy simulation (LES) model. In the observational portion of the paper we present the large-scale conditions that favor the occurrence of the EET (section 3) and address the local external factors controlling temporal and spatial variations of the mean variables during the period (section 4). In section 5 we test how some current parameterizations of surface exchange used in mesoscale models handle observed features of the EET. The main purpose of the discussion of LESs (section 6) is to quantify the extent to which vertical flux divergence, not advection, is the dominant process during EET.

2. Description of the region

A dense network of 26 Portable Automated Mesonet (Brock and Govind 1977) stations operated for 2 months, from 7 September 1982 to 7 November 1982, in the region of Albany, New York. This was part of the FOG-82 project, whose primary goal was to study the conditions that determine radiation fog formation (Meyer et al. 1986).

All stations were within a radius of 15 km from the Albany airport. Almost twenty years after the project it is still not common to find surface observations with such high spatial resolution. The region has moderately complex terrain (Fig. 3), with the distinctive presence of the valleys of two major rivers: the Mohawk and the Hudson. Elevations range from 10 to 140 m above sea level. This is far from extreme topography, such as mountainous landscape (e.g., ASCOT project; Neff and King 1989) or the flatter terrain frequently studied in other projects such as in Kansas (e.g., Haugen et al. 1971). The patchy nature of the Albany area landscape makes this dataset ideal for the study of changes influ-

TABLE 1. Elevation and land use at each station.

Station No.	Elevation (m)	Land use	Station No.	Elevation (m)	Land use
1	85	Ind/For	14	103	Industrial
2	95	Res/Age	15	77	Ind/Agr
3	128	Ind/For	16	84	Agr/For
4	78	Agr/For	17	103	Res/Agr
5	98	Ind/For	18	67	Agr/For
6	120	Residential	19	84	Res/For
7	107	Industrial	20	91	Residential
8	92	Res/Ind	21	98	Agr/For
9	95	Ind/Agr	22	10	Res/For
10	98	Res/Ind	23	65	Agr/For
11	88	Res/For	24	93	Res/For
12	79	Industrial	25	91	Agr/Res
13	116	Residential	26	85	Ind/For

Agr: agricultural; For: forest; Res: residential; Ind: industrial.

TABLE 2. Early evening transition (EET) 19 Sep 1982. Times are local standard time (LST).

Stn. (z)	T inf. pt.	q jump	Station	T inf. pt.	q jump
22 (10)	1815	1818	8 (92)	1741	1740
23 (65)	1820	1811	24 (93)	1832	1750
18 (67)	1828	1809	2 (95)	1837	1837
15 (77)	1830	1808	9 (95)	1831	1830
4 (78)	1745	1746	5 (98)	1852	1800
12 (79)	1914	2032	10 (98)	1802	1801
16 (84)	1842	1840	21 (98)	2020	1808
19 (84)	1815	1844	14 (103)	1758	1726
1 (85)	1831	1831	17 (103)	1944	2030
26 (85)	1830	1825	7 (107)	1849	1851
11 (88)	1828	1800	13 (116)	1913	1729
20 (91)	1855	1751	6 (120)	1748	2031
25 (91)	1828	1820	3 (128)	1850	1829

enced by surface heterogeneity and consequently to an EET study. A remarkable aspect of this period is the establishment of large nocturnal spatial variations (see below).

Urban and rural environments characterize the region and meteorological stations were distributed throughout. It is important to distinguish between commercial/industrial and residential regions as the latter are more vegetated than the former. Table 1 shows the elevation and land use type of each station. Most of the stations, including the urban ones, were located on sites that are more open. In this region, however, it is not possible to find only ''ideal sites,'' nor would such sites be representative. For several stations, sheltering effects are evident in the observations, many times dependent on the wind direction. This difficulty is inevitable, and our view is that it is important to have the effect of obstructions represented in the network, as a typical location in this region as well as in most environments is not open. Quantification of sheltering is done following Fujita and Wakimoto (1982) procedure of finding azimuth-dependent transmission factors (TF), based on the comparison of the mean wind from a given direction at each station with the network maximum average from that direction. An unobstructed direction for a given site has TF = 1, decreasing as shelter effects increase (Fig. 3). Thus, heterogeneity in this network results from three properties of the landscape: topography, land use type, and sheltering.

3. Characterizing the transition

One-minute averaged data are available at each station for temperature, dewpoint, wind, pressure, and maximum wind gust in the minute. The temperature sensor was an aspirated thermistor, humidity was measured by an aspirated wet-bulb thermistor, wind speed by a cup anemometer, and wind direction by a wind vane. Brock and Govind (1977) describe the instrumentation in detail. They also present results from intrument intercomparison, showing that the mean error of the dry-bulb temperature to a reference varied from 0.23° to 0.46°C and for the wet-bulb temperature varied from 0.20° to 0.26°C. All variables were measured at 2 m, except for the winds, measured at 4 m. Six stations (1, 4, 5, 9, 16, and 17) also reported a surface vertical thermal gradient, the 1–4-m temperature difference, which is available from 23 September 1982 to 7 November 1982.

a. Transition nights

Conditions promoting the occurrence of turbulent decay in the early evening are set mainly by large-scale synoptic conditions. Strong responses are favored in postfrontal cases, when large-scale subsidence keeps skies clear and weak winds prevail. Cloud decks reduce radiative cooling, preventing the formation of the SL that initiates decoupling. Twenty out of the 61 nights in the period of observations presented a clear EET. This count does not include intermediate conditions, for which the transition was soon destroyed by increased turbulence, or those for which only some stations experienced a clear transition (detailed in section 3c). In cases of EET, the gust decrease and subsequent strong cooling and q jump are a common feature, observed in most of the network (Fig. 4). The stations with no q jump (3, 6, 13, 14, 17, and 21) (all located in higher terrain) do not experience as strong a gust decrease as does the rest of the network. Similarly, LeMone et al. (2000) observed the smallest q peaks to occur at the highest stations, while the largest ones are in the lowest locations. On a sample night, large variability is observed for the jump times throughout the region (Table 2), pointing to a locally controlled process, which is to be expected, given the small eddy size that dominates turbulent motions during the period. There is close agreement between the times of q jump and the T temporal inflection point at individual stations on this night. In fact, at 12 stations, these two events occur within 10 min of each other and the largest timing differences occur at those higher stations that do not exhibit a clear

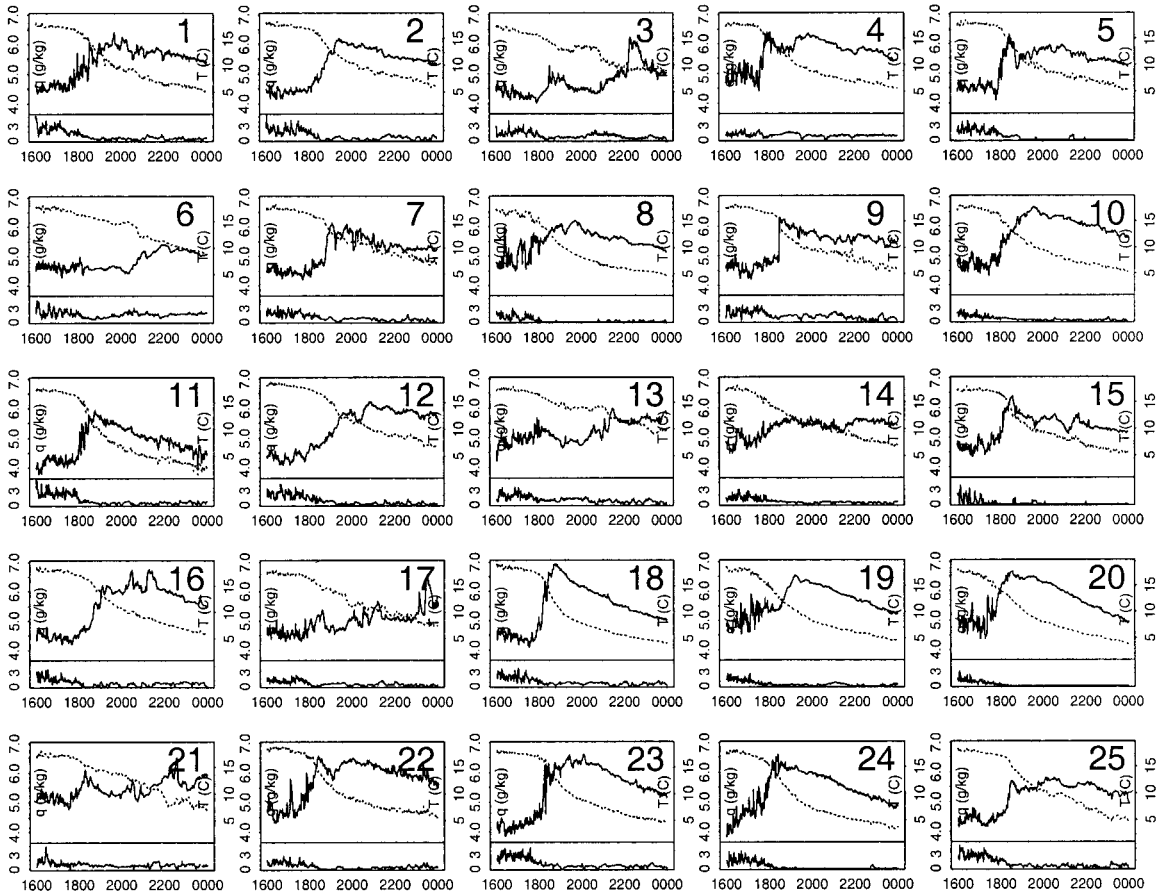

FIG. 4. Each frame represents the evolution of specific humidity (upper panels, solid), temperature, (upper panels, dotted) and wind gusts (lower panels) at one station for the night of 19 Sep 1982. The station numbers are shown in the upper right side of the frames. Locations are given in Fig. 3.

transition. The agreement between the times of q jump and inflection point in temperature suggests that simple measurements from thermographs can provide information on the timing of turbulence decay at the surface (FL89). Spatial variability of time and magnitude of the jumps is a fundamental aspect of the EET and in the next section we address the factors controlling this phenomenon.

Spatial variability of temperature for the entire night is largely determined during EET (Fig. 5). As turbulence decays in the surface layer, local features exert a stronger control on the mean quantities, causing a big spatial variability of temperature ($\sigma_{T,\text{spat}}$, Fig. 5, lower panels). A sharp increase in $\sigma_{T,\text{spat}}$ occurs during the EET, reaching values of 2.5°C and remains large through the night. A peak in $\sigma_{T,\text{spat}}$ occurs at the end of the EET. Afterward it decreases (11 September and 28 October) or remains approximately constant (5 October), even though temperature values at all stations are still falling. On 5 October the temperature spread starts to drop after the transition, as on the other nights. The sudden increase observed in the middle of the night is a consequence of the restart of turbulence in some stations, evidenced by the increased wind gusts. As turbulence dies, temperature spread drops again.

At a single point, the transition can be determined by the time it takes for the wind gust to decay from mid-afternoon values. This transition time can be as long as 1 or 2 h (see Figs. 1 and 4), and varies greatly from station to station. To define the EET in the network, we concentrate on the period that begins with the sharp increase in temperature spread and ends when the spatial standard deviation reaches its maximum (dotted vertical lines in Fig. 5).

Large spatial variability of nighttime surface temperatures on clear nights is a well-known feature (Geiger 1971; Fitzjarrald and Moore 1994; Gustavsson et al. 1998). At EET, surface decoupling likely allows local circulations to develop, causing the downslope flow of cold air, leading to enhanced spatial temperature variability. Whereas during the day the coupling determines uniformity of the directions as determined by large-scale forcing, the nocturnal local winds come from different directions at each station, determined by the moderately complex topography of the region. It causes the spatial standard deviation of wind direction to increase at EET

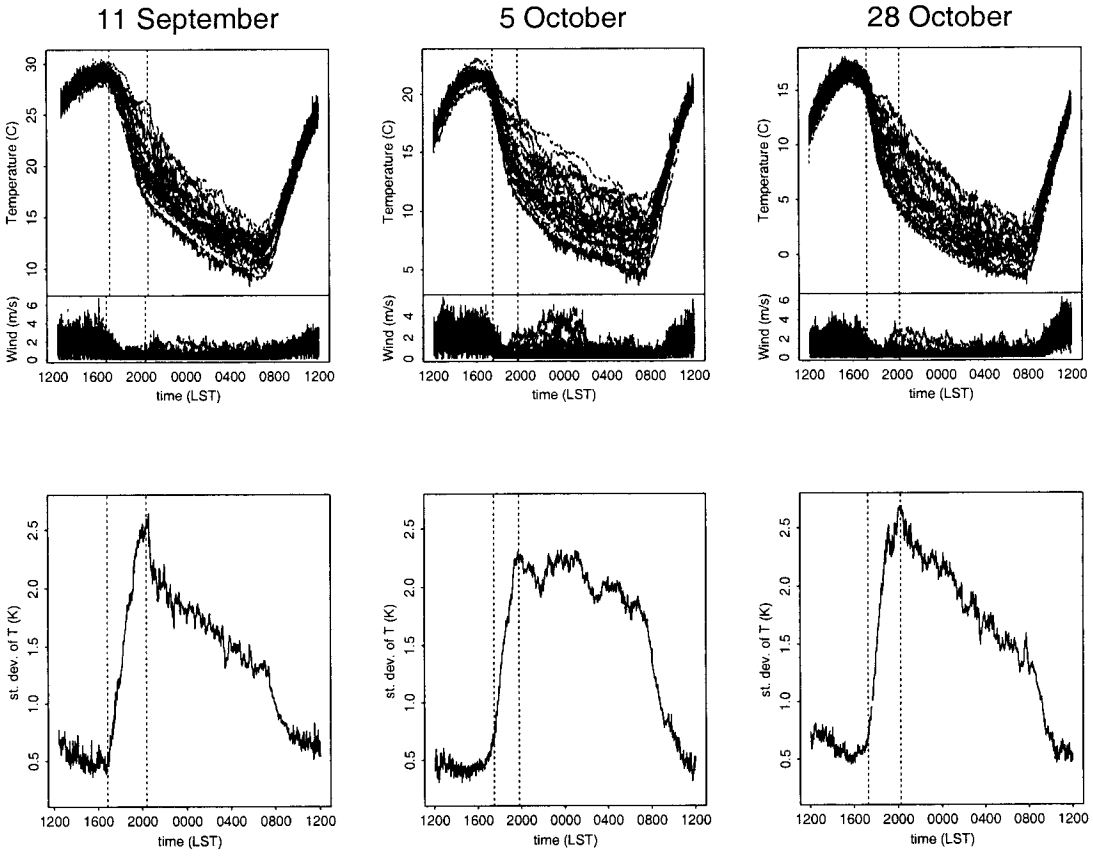

FIG. 5. Upper row: temporal evolution of temperature (upper panel) and wind gusts (lower panel) at the 26 stations for three different nights. Lower row: $\sigma_{T-\text{spat}}$ for each of the nights shown in the upper row.

(Fig. 6). Mahrt (1981), looking at tower data from different vertical levels, observed a clockwise turn of the wind at early evening as a consequence of the increased importance of the flux convergence term in the momentum equation. This is not apparent at the surface in our dataset, where the switch from large-scale driven wind direction to a topographically driven one does not show a preferential direction to occur. Similarly, Caughey et al. (1979) could not find consistency in the direction surface winds turned at EET.

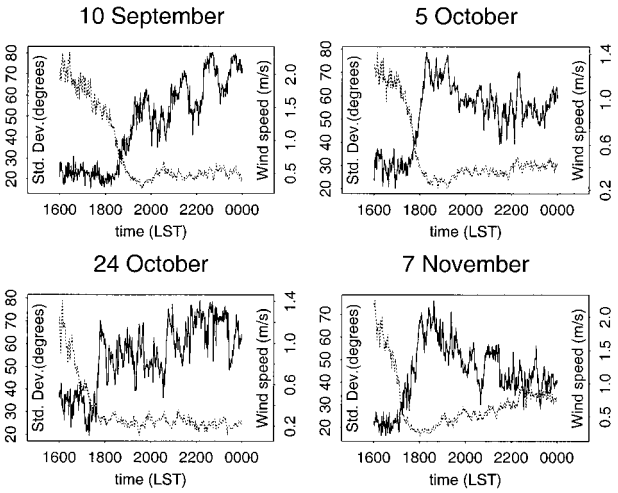

FIG. 6. Spatial standard deviation of wind direction (solid) and mean wind speed (dotted) for four different nights.

The two necessary conditions for an EET and the consequent large surface spread of mean variables are clear skies and weak winds. In fact, these two are dependent, since in most cases the latter is a consequence of the former. We tested sensitivity to nocturnal cloudiness using hourly sky cover reported at the Albany airport (National Climatic Data Center surface airways database). The early evening spatial variation of temperature is maximized under clear skies and light winds (Fig. 7). More uniform temperatures arise when either of the conditions is not met. Distinction is only achieved when using the ''opaque sky cover observations,'' rather than ''total sky cover'' (not shown), suggesting that low and medium clouds have a stronger effect on the EET than do high clouds.

b. Nontransition nights

On some nights, no well-defined EET occurs (Fig. 8). In these cases, the presence of high winds in the

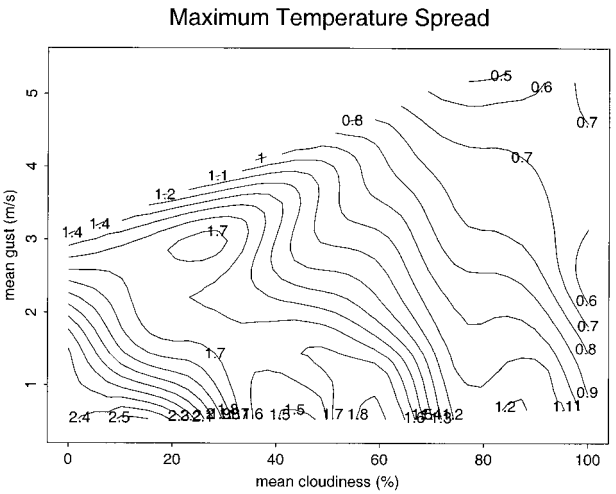

FIG. 7. Smoothed contours of maximum spatial standard deviation of temperature for different values of opaque cloud cover and mean wind gusts. Cloud cover observations are made at Albany airport, close to station 1. Mean values of cloud cover for the night are considered.

entire period keeps the surface coupled to higher levels. The coupling has the important consequence of spatially homogenizing the surface conditions. In the three cases shown in Fig. 8, $\sigma_{T,\text{spat}} < 1.2$°C. Winds remain driven by their synoptic-scale forcing rather than by local conditions. Cold air drainage flows are not likely to be initiated and, although the surface experiences nocturnal cooling, it is more spatially uniform.

c. *Partial transition nights*

In 4 out of the 62 nights, the transition occurred at some stations but not at others. For these cases most of the stations follow the behavior of a nontransition night, with uniform cooling (Fig. 9, upper left panel). A small number of places experience a stronger temperature decrease during portions of the night. Data from three stations illustrate this behavior. Station 3, at a hilltop, is a typical case of nontransition, with intense turbulence and not much cooling through the night. Stations 18 and 22 (in valleys), however, experience quite strong cooling for parts of the night, clearly associated with the reduction of turbulent activity and subsequent disconnection at these periods. At station 18, the transition was well defined a little after 1800 LST, with temperature decrease and specific humidity jump. At 2000 LST this station was almost 6°C colder than most of the network. Turbulence built up again a little after this hour and an intense warming was experienced, bringing its temperatures together with the rest of the network. Similar situations are observed at station 22. The buildup of turbulence is accompanied not only by temperature increase, but also by a specific humidity drop, which is a consequence of stronger mixing activity. In this situation, often decoupling happens at only one station. This is a different form of surface spatial variability, in which single locations have completely distinct features from those of their surroundings. It is a good illustration of the effects of turbulent intermittence in the boundary layer variables. The disconnection happens preferentially at those colder stations where the inversion and subsequent TKE destruction is more intense. Thus, the prediction of the decoupled locations in these cases depends on understanding the processes that control the spatial distribution of nighttime temperatures (section 4c).

4. Physical processes controlling the EET

Mean temperature and specific humidity at EET are given by

$$\frac{\partial \overline{\theta}}{\partial t} = \underset{(1)}{\text{ADV}_\theta} - \underset{(2)}{\frac{\partial \overline{w'\theta'}}{\partial z}} - \underset{(3)}{\frac{\partial R_n}{\partial z}}$$

$$\frac{\partial \overline{q}}{\partial t} = \underset{(1)}{\text{ADV}_q} - \underset{(2)}{\frac{\partial \overline{w'q'}}{\partial z}}, \qquad (2)$$

where term 1 represents the sum of advective contributions (ADV), term 2 is turbulent vertical flux divergence, and term 3 is the radiative flux divergence.

We hypothesized that the q jump and T inflection point are the consequence of an enhancement in term 2, caused by the confinement of mixing activity to a shallow layer next to the ground. In this section we address how sheltering and topography affect the changes observed in the mean variables. This analysis will be helpful to understand the relative roles of terms 1 and 2. Later, in session 6, we explicitly compare these terms.

a. *Effects of topography and sheltering*

To understand the role topography and sheltering [estimated here by the transmission factors (TFs), shown in Fig. 3] play on the mean variables at EET, we made composites of the 20 transition cases. On each night, we considered the transition to occur from the start of increase in spatial standard deviation of temperature until it peaks (dotted lines in Fig. 5). This period was divided into 100 intervals to form composites of the evolution of wind gust, dq/dt and dT/dt. Finally, we arranged these time series according to height of the station and TF for the afternoon wind direction for each station.

Wind gusts tend to persist longer at higher stations (Fig. 10a), but the timescale for wind decay seems to be the same for any height value between 70 and 110 m. In contrast, the gust decay occurs for any value of TF, but tends to occur earlier at sheltered locations (Fig. 10b). On average, the gusts at stations with TF approximately 0.2 collapsed to 20% of the maximum value in

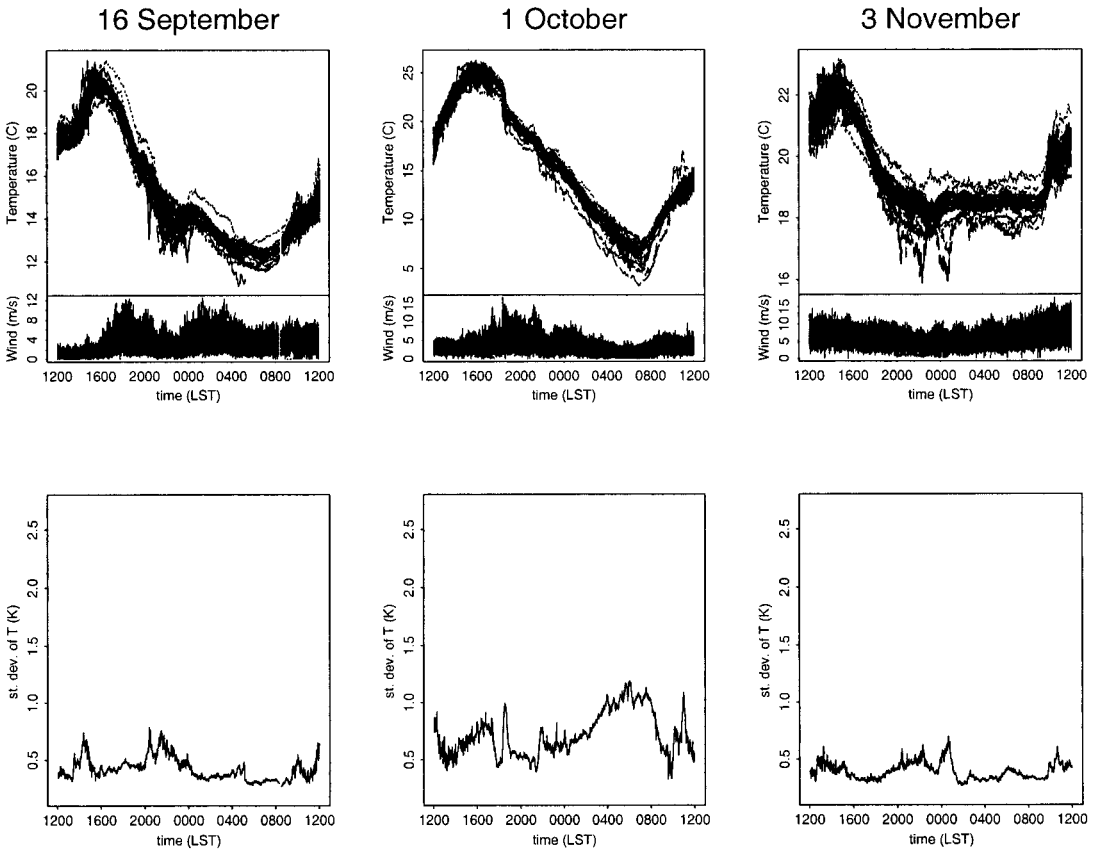

FIG. 8. Upper row: temporal evolution of temperature (upper panel) and wind gusts (lower panel) at the 26 stations for three different nights. Lower row: $\sigma_{T,\text{spat}}$ for each of the nights shown in the upper row. The vertical scale is the same as in Fig. 5, for comparison.

the 20% of the transition. At the same time, the wind has decayed only to 60% of its maximum at a perfectly open location (TF = 1). The consequences of these two effects on the q jump can be seen in Figs. 10c and 10d. The largest jumps occur at intermediate values of TF and lower locations. This is because higher stations do not experience a full transition as the wind decay is reduced there. At the same time, highly sheltered stations do not have sufficient turbulent fluxes to produce q jumps. Even though no temporal trend is apparent with topography, it is clear that more sheltered stations experience an earlier jump than do those at more open sites, a direct consequence of the more rapid wind decay at obstructed places. This also holds for the jump magnitudes, which peak for a value of TF close to 0.7. Apparently this value optimizes conditions for jump occurrence, with enough turbulent intensity to promote mixing with the surface, but not so much as to keep the surface and upper levels connected, inhibiting the transition. Interestingly, the same trends are not observed for the cooling rates, despite the agreement between the time when they occur with the time of q jumps, shown in Table 2. Rather, the time of maximum cooling rate tends to be always around 25% of the transition, for any value of TF and topography (Figs. 10e and 10f). The only limiting factor here seems to be the location at high places, which inhibits strong cooling.

Both q jump and time of maximum cooling rate always happen in the first half of the transition. The EET can then be subdivided into two periods: the first, when most of the temporal variations happen, and a second when turbulent fluxes decrease in magnitude. In this second period the variables and their spatial distributions are still varying, but to a smaller degree.

b. Richardson number evolution

Using the temperature difference between 1 and 4 m, available at six stations, we can estimate the evolution of an appropriate bulk Richardson number $\text{Ri}_b = h(g/\Theta)(T_4 - T_1)/(u^2 + v^2)$ during the EET (Fig. 11). Here u and v are the wind components, and h is 3 m, the difference between the two levels. A nearly exponential increase of Ri_b is observed at all six stations. Places with higher rates have a tendency to earlier jumps.

These observations can be explained theoretically by looking at the prognostic equation for the Richardson number (Ri):

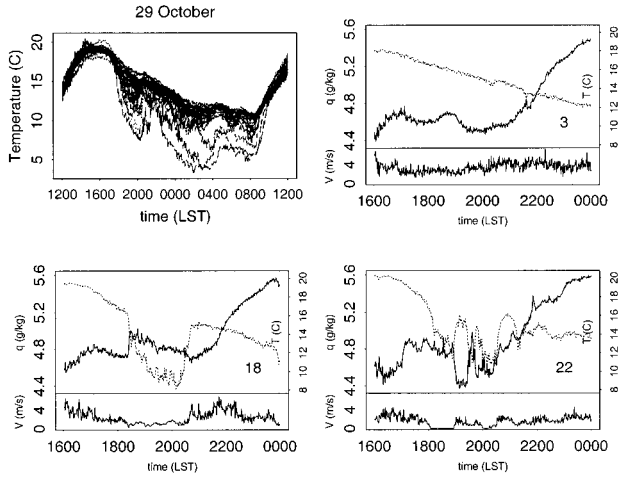

FIG. 9. Upper left frame shows the evolution of temperature at the 26 stations. Other frames show specific humidity (upper panel, solid), temperature (upper panel, dotted), and wind gusts (lower panel) at three different stations. The station number is shown in the lower right corner.

$$\frac{\partial(\mathrm{Ri})}{\partial t} = \frac{\partial}{\partial t}\left(\frac{\frac{g}{\Theta}\frac{\partial\theta}{\partial z}}{S^2}\right) = \frac{1}{S^2}\frac{g}{\Theta}\left[S^2\frac{\partial}{\partial z}\frac{\partial\theta}{\partial t} - 2S\frac{\partial\theta}{\partial z}\frac{\partial S}{\partial t}\right], \quad (3)$$

where the term involving the time variation of Θ was neglected and S is the mean shear, defined as

$$S = \sqrt{\left(\frac{\partial U}{\partial z}\right)^2 + \left(\frac{\partial V}{\partial z}\right)^2},$$

and all the other variables follow standard notation. Substitution of Eq. (2) into (3) leads to

$$\frac{\partial \mathrm{Ri}}{\partial t} = \frac{\mathrm{Ri}}{S}\left[\frac{m(m-1)}{h^2}u_*^2 - 2\frac{\partial S}{\partial t}\right] + \frac{g}{\Theta S^2}\frac{\partial^2(R_n)_0}{\partial z^2}, \quad (4)$$

where a generalized form of the vertical profile parameterization for the sensible heat flux by Grant (1997) was used: $\overline{w'\theta'} = (1 - z/h)^m(\overline{w'\theta'})_0$ and that $(\overline{w'\theta'})_0/u_*^2 = (\partial\theta/\partial z)/S^2$. Here, h is the height at which the turbulent fluxes go to zero.

The radiative flux term is the forcing that first makes the surface layer stable, causing the transition of Ri from negative to positive. When Ri becomes positive, the first term in Eq. (4) leads to the exponential increase and the radiative term, essential at the start of the transition, loses its relative importance. The rate of the exponential increase of Ri after sunset is then given by the two terms inside the brackets in Eq. 4. Both are positive in the first part of the transition (when the wind and, subsequently, S are decaying). The effect of obstructions that cause more rapid wind decay is represented by the second term inside the brackets, and this determines the higher rates of increase observed at sheltered locations. Once turbulence diminishes, the terms inside the brackets vanish and Ri only increases slowly due to radiative effects. Eventually, if turbulence builds up again, the second term in the brackets becomes negative, causing the decrease of Ri.

c. Horizontal inhomogeneities in cooling rates

In this region, the end of the EET is the time of maximum horizontal variability in temperature in the daily cycle (Fig. 5). For different evenings for which there is disconnection, the spatial pattern of surface temperatures at this moment is very similar. The coldest places always tend to be the same ones, as do the warmest.

To compare different nights, with different mean temperatures and spatial variabilities, we define a ''spread factor'' (SF), which indicates by how many standard deviations the temperature at a given location is above or below the network average: $\mathrm{SF} = (T - \langle T\rangle_{\mathrm{spat}})/\sigma_{T,\mathrm{spat}}$. Here, $\langle T\rangle_{\mathrm{spat}}$ is the spatial average for the network and $\sigma_{T,\mathrm{spat}}$ is the spatial standard deviation. There is no simple relation between SF and elevation (Fig. 12a). The three highest stations are also the warmest, but no conclusions can be drawn for the remaining locations. Land use does not seem to explain the variability, and, except for station 12 (urban), urban stations tend to be colder than rural ones at similar elevations, which is a counterintuitive result.

Harrison (1971) showed that a linear relation between minimum temperatures and height is found if not the absolute height but the distance from valley floor is considered. Geiger (1971, p. 393) also suggested that relative elevations control the nighttime temperature. In our network there is a good linear relation between temperature at the end of the EET and the local relative elevation. This is defined here as difference between station height and the mean height in an area of 3 km $\times$ 3 km centered at the station ($z - mz$, Fig. 12b). Some spread still persists and we hypothesize that this can be due to the different types of land use practices in the network. Urban stations tend to be warmer than rural ones located at similar ranges of $z - mz$. This result is opposite to what was observed in Fig. 12a. The explanation for the difference here is that urban regions usually coincide with valleys, and are thus colder than the rural locales if the topographical correction used in Fig. 12b is not used. The value of 3 km was the one for which the best correlation was found between SF and ($z - mz$). It suggests that the temperature at a given point is affected by drainage processes within an area of 3 km $\times$ 3 km around that location.

5. Two-layer model

McNider et al. (1995) used a simple two-layer model to assess the predictability of surface variables in the parameterizations used in mesoscale models for the surface exchange. They found that very different results arise depending on whether the upper layer is connected

to the surface or not. We noted earlier that this connection has a large effect on mean quantities at the surface, in the form of a q jump and inflection point in the temperature time series. In addition, timing and magnitude of these processes are strongly affected by surface characteristics such as topography and sheltering. The data described in sections 3 and 4 come from an area of 20 km $\times$ 20 km, similar to the size of a single grid cell in a mesoscale model. One consequence is that for a model to be able to simulate properly the state of coupling between the surface and the upper boundary layer, it must describe the strong subgrid spatial variability observed in the case of turbulence decay.

The exchanges between the first and second layer of the model and between the surface and first layer are determined by stability parameters, in the form of Richardson numbers. Thus, in this parameterization, the vertical flux divergence is the relation between these two exchanges. In this section, we use the McNider et al. (1995) set of equations to assess if this kind of representation of the vertical flux divergence is able to properly represent the behavior of the mean quantities at the EET.

We included moisture and shortwave radiation in the McNider et al. (1995) equations and started the runs when shortwave radiation is at its peak to see if the EET is well resolved by the model. The prognostic equations are

$$\frac{du_1}{dt} = f(v_1 - v_g) + \frac{1}{z_{3/2} - z_{1/2}}\left(\frac{K_{m3/2}(u_2 - u_1)}{z_2 - z_1} - u_* \cos(\Psi)\right), \quad (5)$$

$$\frac{dv_1}{dt} = f(u_g - u_1) + \frac{1}{z_{3/2} - z_{1/2}}\left(\frac{K_{m3/2}(v_2 - v_1)}{z_2 - z_1} - u_* \sin(\Psi)\right), \quad (6)$$

$$\frac{d\theta_1}{dt} = \frac{1}{z_{3/2} - z_{1/2}}\left(\frac{K_{h3/2}(\theta_2 - \theta_1)}{z_2 - z_1} - u_*\theta_*\right), \quad (7)$$

$$\frac{dq_1}{dt} = \frac{1}{z_{3/2} - z_{1/2}}\left(\frac{K_{q3/2}(q_2 - q_1)}{z_2 - z_1} - u_* q_*\right), \quad (8)$$

$$\frac{d\theta_g}{dt} = \frac{1}{C_g}(K\downarrow + L\downarrow - L\uparrow - H_0 - \mathrm{LE}_0). \quad (9)$$

We assume that $K\uparrow$ is a constant fraction of $K\downarrow$ (and is included in its parameterization). Here, indices 1 and 2 refer, respectively, to first and second layer ($z_1 = 5$ m and $z_2 = 50$ m), with fractional numbers referring to intermediate levels. The geostrophic wind components are given by u_g and v_g and Ψ is the direction of the surface wind [$\Psi = \arctan(v_1/u_1)$]. Turbulent mixing is switched on or off depending on the value of the Richardson number. The critical Richardson number (often taken to be $\mathrm{Ri}_c = 0.25$) is a value above which no turbulence exists as all mechanical production is destroyed by the stable stratification:

$$f(\mathrm{Ri}) = \begin{cases} (1 - \mathrm{Ri}/\mathrm{Ri}_c)^2 & \mathrm{Ri} < \mathrm{Ri}_c \\ 0 & \mathrm{Ri} \geq \mathrm{Ri}_c, \end{cases} \quad (10)$$

$$u_* = k\sqrt{f(\mathrm{Ri}_{1/2})}\sqrt{u_1^2 + v_1^2}/\ln(z_1/z_0), \quad (11)$$

$$\theta_* = k\sqrt{f(\mathrm{Ri}_{1/2})}(\theta_1 - \theta_g)/\ln(z_1/z_0), \quad (12)$$

$$q_* = k\sqrt{f(\mathrm{Ri}_{1/2})}(q_1 - q_g)/\ln(z_1/z_0), \quad (13)$$

$$K_m = K_h = K_q = f(\mathrm{Ri})\kappa z S, \quad (14)$$

where S is the wind shear.

The vertical temperature profile is controlled by a simple surface energy budget [Eq. 9], where $K\downarrow$ follows a sinusoidal form, going to zero at sunset. The longwave radiative terms are given by

$$L\downarrow = \sigma[Q_c + 0.67(1 - Q_c)][(1670Q_a)^{0.08}]\theta_2^4, \quad (15)$$

$$L\uparrow = \sigma\theta_1^4, \quad (16)$$

where Q_c is the cloud cover and Q_a is the specific humidity at the upper boundary layer. For simplicity, we assume the surface emissivity is unity. The turbulent heat fluxes are

$$H_0 = -\rho C_p u_* \theta_* \quad \text{and} \quad \mathrm{LE}_0 = -\rho C_p u_* q_*. \quad (17)$$

Further details on the set of equations can be found in McNider et al. (1995). Figure 13 shows that lower temperatures (consequence of the turbulence decay) depend on clear skies and light geostrophic winds, a result qualitatively similar to what observations show (Fig. 7). The vertical lines in the lower portion of Fig. 13 show the dependence of the equilibrium temperature on cloud cover. Model results are insensitive to the magnitude of the geostrophic wind as long as the surface and upper layers are decoupled.

Solutions of McNider's model for different values of geostrophic wind (Fig. 14) show an inflection point in the temperature series, a smooth maximum in dq/dt (rather than a sharp q jump), and u_* decrease in the early evening. The strong surface cooling and moistening is a consequence of the enhanced vertical flux divergence, as the exchange between the first and second layer of the models decreases at a faster rate than the one between the ground and the first layer. Different results (higher equilibrium q and T) are found if the geostrophic wind is strong enough to keep the connection between the layers.

The simple parameterization is able to resolve some important features of the EET at a single point. It responds properly to the effects of cloud cover, strong winds, and the enhancement of vertical flux divergence. The evolution of moisture and temperature shown in Fig. 14 qualitatively resembles that observed at many stations (Fig. 4). Those stations experiencing a full tran-

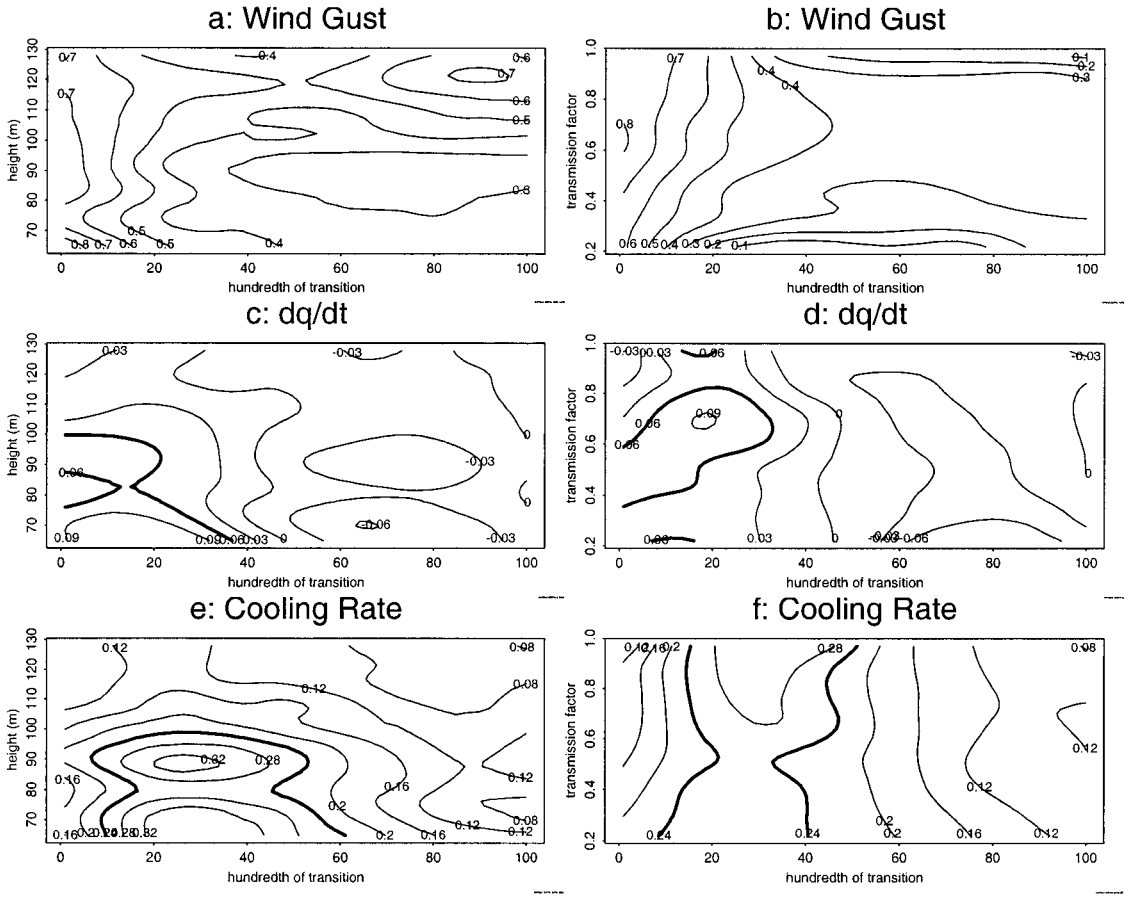

FIG. 10. Composites of wind gust, dq/dt and dT/dt for the EET period, defined in the text. Each series was normalized by its maximum value. The results organized by (a), (c), (e) elevation of the station or (b), (d), (f) transmission factor (TF), averaged and smoothed. TF depends on the afternoon wind direction at the station, defined as the mean direction from 1600–1800 LST (period preceding the transition). TF is the mean value in a sector of 60° centered on this direction. Contour labels show values of the variables relative to their maximum.

sition can be associated with the cases of weak geostrophic wind in Fig. 14 and those that remain connected along the transition (higher stations) can be associated with the curve of $u_g = 9$ m s^{-1}. A remaining problem is to explain the strong spatial variability of the observations. The different temperature evolutions shown in Fig. 14 are a consequence of a wide range of large-scale winds in the model. However, Fig. 5 shows that in the real world, surface heterogeneities can be enough to cause a similar range of temperature evolutions to be observed at the same period in different points of a region as small as a single grid cell of a mesoscale model. Accuracy of forecasts of minimum temperature and scalar concentrations at nighttime are thus strongly affected by the local character of EET processes.

6. Large eddy simulations (LES) of the EET

In sections 3 and 4, we showed the strong variation to which temperature and specific humidity are subject to during the EET. Observations show that sheltering controls the onset time and magnitude of the transition in moisture, but does not seem to have strong influence on temperature. Rather, this variable tends to follow local topographic features. It indicates that thermal advection is more important to the heat budget during the transition than moisture advection is to the q budget. In this section, we perform LES of the EET for a gently sloping terrain, with the purpose of comparing the magnitudes of vertical flux divergence and advective terms for both q and T.

The model used in this work has been described in Smolarkiewicz and Margolin (1997). Here, we will give only a brief explanation of the equations used:

$$\frac{d\mathbf{V}}{dt} = -\nabla\pi + \mathbf{k}g\frac{\theta}{\theta_0} + \mathbf{D}_v, \tag{18}$$

$$\nabla(\bar{\rho}\mathbf{V}) = 0, \tag{19}$$

$$\frac{d\theta}{dt} = D_\theta, \tag{20}$$

where (18) is the momentum equation, (19) is the continuity equation, and (20) is the thermodynamic equa-

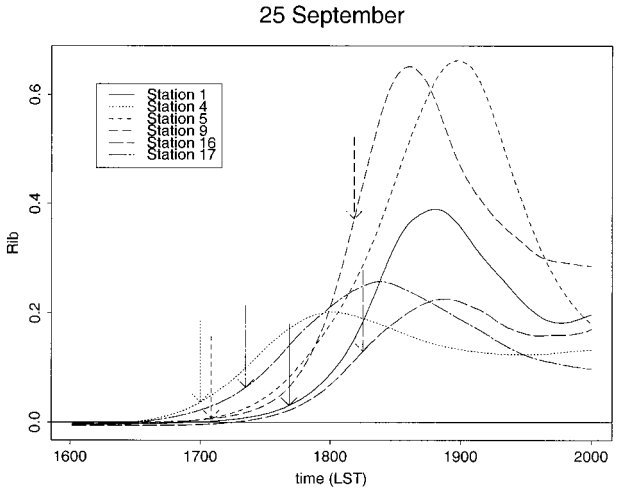

FIG. 11. Smoothed bulk Richardson number (Ri_b, defined in text) evolution at six stations, as given by legend. Arrows point the time of maximum dq/dt.

tion. Here, $d/dt \equiv \partial/\partial t + \mathbf{V} \cdot \nabla$, $\mathbf{V}$ is the velocity vector, θ the potential temperature, ρ is density, and π is pressure perturbation with respect to the undisturbed environmental profile normalized by anelastic density. The terms denoted by D represent the LES subgrid-scale parameterization, described in detail by Sorbjan (1996).

The purpose of these simulations is to understand the role of flux divergence close to the surface at EET. We generate a convective boundary layer (CBL) that will be cooled from below at a second stage. Nieuwstadt and Brost (1986) and Sorbjan (1997) performed simulations using the same type of LES. However, they were interested in understanding the decay of turbulence in the remnant CBL, a neutral layer decoupled from the surface.

The domain has 32 points in each of the horizontal directions and 251 in the vertical, with 50-m spacing in the horizontal and 4 m in the vertical. The time step is 1 s. The model equations are integrated in time using the Adams–Bashforth scheme, with the advection terms determined by Eulerian finite-difference approximations (Smolarkiewicz and Margolin 1997). The lateral boundary conditions are periodic both in x and y. At the upper boundary a rigid lid is assumed.

The convective simulations are started with a neutral potential temperature profile up to the height of 300 m. Above that, an inversion of 2.5 K km^{-1} is assumed. The initial moisture profile is uniform, at 5 g kg^{-1}. These simulations ran for 40 000 time steps (11.1 h). At the surface a constant sensible heat flux of 10 W m^{-2} and a latent heat flux of 63 W m^{-2} were assumed. This was the latent heat flux necessary to promote the change in moisture observed in the boundary layer from 1200 to 0000 UTC of the next day, as given by the soundings for Albany, at 5 October 1982. After the end of the CBL run, the EET runs for a total of 18 000 time steps (5 h).

The radiative processes at the surface are parameterized in the manner suggested by McNider et al. (1995), as described in section 5. We want to realistically simulate the transition, but retain a simple radiation treatment. This way, in contrast to Nieuwstadt and Brost's or Sorbjan's arbitrary forcing of the turbulent heat flux evolutions, in our simulations the nocturnal cooling and all subsequent processes are a more natural response to diminishing solar radiation at sunset. We consider the first level of the model to be at z_0, the roughness height, and define a variable θ_g (ground temperature). The time evolution of θ_g responds to the surface budget, described in the previous section [equations (9), (15), and (16)]. To maintain the convective condition for a time before night falls, $K\downarrow$ only goes to zero after 10 000 time steps (2.8 h).

In the model, radiative forcing only exists at the surface, where it affects θ_g [Eq. (9)]. Radiative flux divergence is neglected and the surface cooling is transferred to the adjacent air via the vertical turbulent flux divergence. Not considering radiative flux divergence here is supported by two facts. First, it has little relative importance at EET, a short period during which the turbulent flux divergence is largest. Second, we note that one of our major interests here is to understand horizontal variability. Radiative flux divergence has only a small tendency to homogenize the variables horizontally, as can be seen in Fig. 5, where $\sigma_{T,\text{spat}}$ decreases late at night, when this term is dominant.

The turbulent heat fluxes in (9) are determined by a linearization of the bulk form: $\tau_{\psi w} = C_\psi V_1(\psi_s - \psi_1)$, suggested by Glendening (1996):

$$\tau_{\psi w} = \|\tau_{\psi w}\|\left[\frac{(\psi_s - \psi_1) - \|\psi_s - \psi_1\|}{\|\psi_s - \psi_1\|} + \frac{V_1}{\|V_1\|}\right], \quad (21)$$

where double vertical bars represent spatial average over the domain, and ψ is a generic variable. The bulk coefficients (C_ψ) are assumed constant, as the first level (z_1) is close to the surface, making $z_1/|L|$ (where L is the Obukhov length) small enough so that the neutral values of C_ψ can be used.

The surface specific humidity is taken as the minimum between the initial value and $q_{\text{sat}}(\theta_g)$. The initial values of θ_g and q_g are given by the value at the end of the convective run at the first level of the model, incremented, respectively, by 1 K and 1 g kg^{-1}, so that the EET fluxes are initialized positive. This arbitrary action is necessary to initialize the ground variables, which do not exist in the CBL runs. We performed 2D sensitivity tests to the initial conditions on q_g, finding that the main results of the simulations are not affected. A mean wind of 1 m s^{-1} is imposed at the top of the domain.

To assess the importance of flux divergence relative to horizontal advective process at EET, the idealized topography used resembles a bowl, lower in the middle than at the borders. Due to the cyclic boundary con-

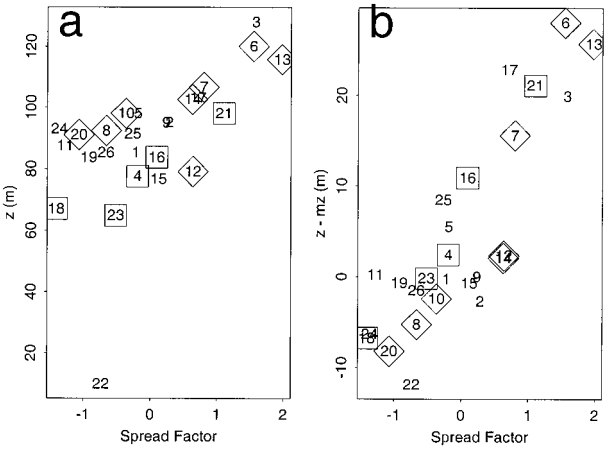

FIG. 12. (a) Relation of the temperature spread factor (see text) with elevation; (b) temperature spread factor vs the difference between station elevation (z) and mean height of a 3 km × 3 km area (mz) centered on the station. Squares indicate rural stations, and diamonds are urban ones. Stations with no symbol are located in mixed environments. The numbers identify the different stations.

ditions, it is more realistic to say that the domain consists of a mosaic of bowls arranged side by side, horizontally (Fig. 15). The variation is gentle, 10 m from bottom to top, but enough to produce differential horizontal cooling.

Much colder temperatures are observed in the center than at the borders, pointing to the expected pattern of cooling (Fig. 16). Temperature and specific humidity organize according to topography as the transition goes on (Fig. 17). A cold pool develops, well defined after 4 h of simulation, becoming larger and more intense after 5 h. Specific humidity jumps are observed at the same time (around 2.5 simulation hours, before model sunset) throughout the network. The pattern of higher

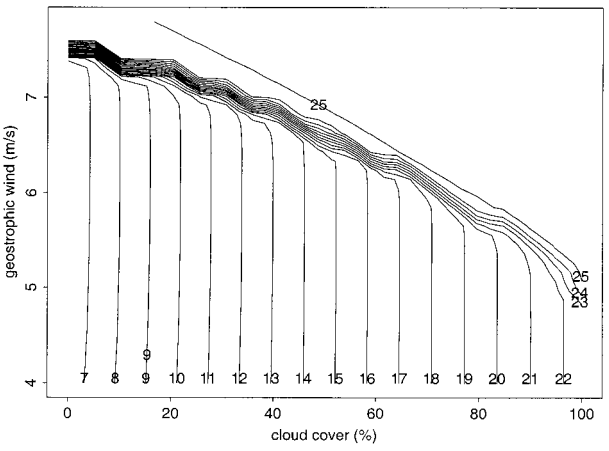

FIG. 13. Final temperature of the McNider et al. (1995) two-layer model as a function of cloud cover and geostrophic wind. Initial temperature was 300 K (26.85°C). The region with high density of contour lines represents the boundary between connection and disconnection.

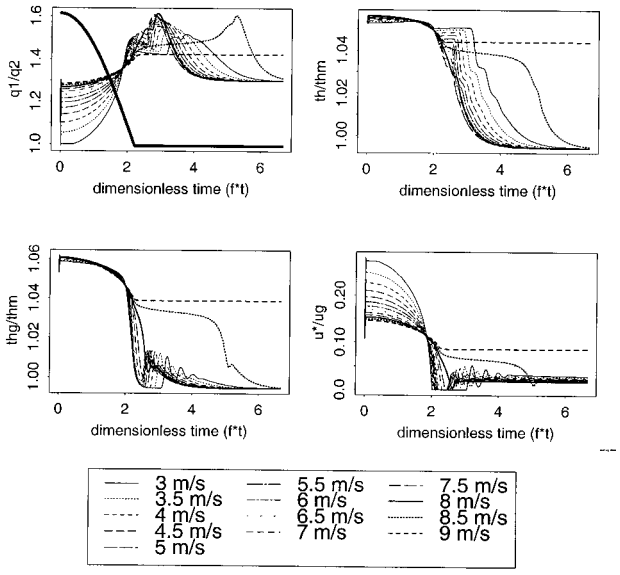

FIG. 14. Dimensionless solutions of McNider et al. (1995) two-layer model for different values of geostrophic wind, as given by legend. Solid line shows shortwave radiation, determining the moment of sunset. Here, q_1 and q_2 are specific humidity at the first and second layer, respectively, thg is ground temperature, th is first level temperature, thm is the temperature above the second layer, and f is the Coriolis parameter. The reference values q_2 and thm are constants (6 g kg^{-1} and 285 K, respectively). The thick line in the upper-left frame is the downward short-wave radiation.

q in the valley and smaller q at the higher places only develops after the jump occurrence.

The wind field is also affected by the onset of the EET, as shown in Fig. 18. The 4-m wind magnitude [level of wind observations in the portable automated mesonet (PAM) network] shows a dependence on the elevation as the surface inversion builds. The pattern is symmetrical in y, but not in x, the direction of the mean winds. The highest magnitudes are not observed at hill-

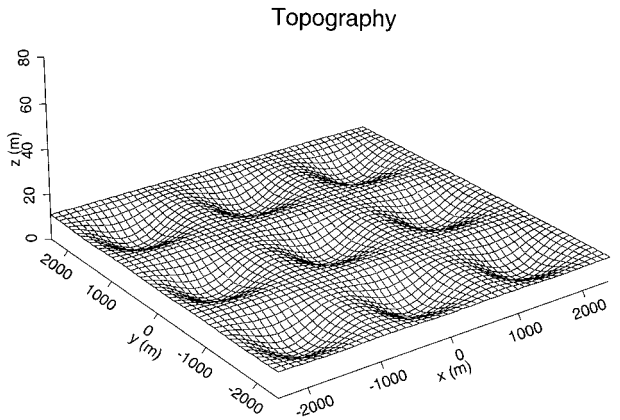

FIG. 15. Topography of the domain, used in the LESs. Vertical scale is exaggerated. The actual simulation domain consists of only one of the bowls shown here. The mosaic is shown to characterize the effect of the cyclic lateral boundary conditions.

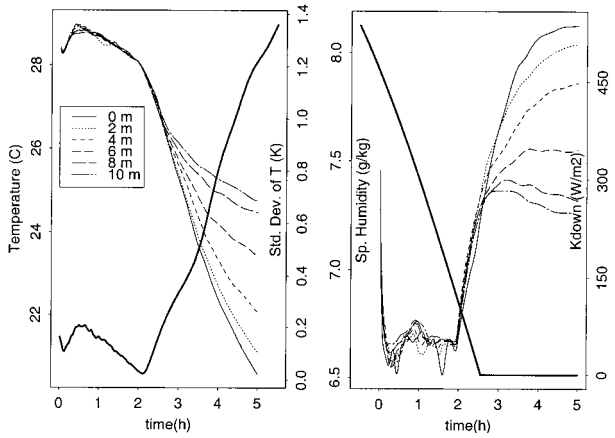

FIG. 16. Simulated evolution of (left) temperature and (right) specific humidity for different elevations, as given by legend. The class of each point is the one nearest to its actual elevation, with 0 m being at the bottom of the valley, and 10 m at the ridges. Thick line in left frame is the spatial standard deviation of the temperature and in the right frame is the downward shortwave radiation (scales in the right sides).

tops, as supported by theory (Kaimal and Finnigan 1994, p. 175), but on the slopes, where the drainage effects are pronounced. The cold pool causes a region of large gradient of wind magnitude (Fig. 18, lower frames), but only on the side where the downslope flow tends to accelerate the mean wind. The region of calm air increases in size from the 4-h observation to the 5-h, as the inversion grows in the period.

Since we are neglecting radiative flux divergence, the only sink of temperature is determined by the surface radiative cooling. Vertical turbulent flux divergence is the physical process responsible for cooling the adjacent air and this cold air is later transported to other regions by advection. Thus, advective effects and vertical flux divergence are the dominant processes in the temperature and specific humidity tendency equations at all times. For temperature, a broad, negative early peak in the vertical flux divergence term is evident (Fig. 19a), related to the maximum cooling rate. The magnitude of maximum cooling rates due to flux divergence does not vary greatly around the network, tending to be around -0.08 K s^{-1}. In contrast, advective processes do not show a clear peak at any given time (Fig. 19b), presenting larger variations along the period. Advection does seem to play an important role in the differential cooling, however. This fact is especially true in the last 3 h of the simulation. During this period, positive advection at the higher places and negative advection in the valley are related to the downslope flow of colder air. In fact, at the lower region of the domain, negative advection is stronger than the cooling due to the vertical flux divergence.

There is an early peak in vertical flux divergence (Fig. 19c), related to the q jump, is clear. In the model, it is

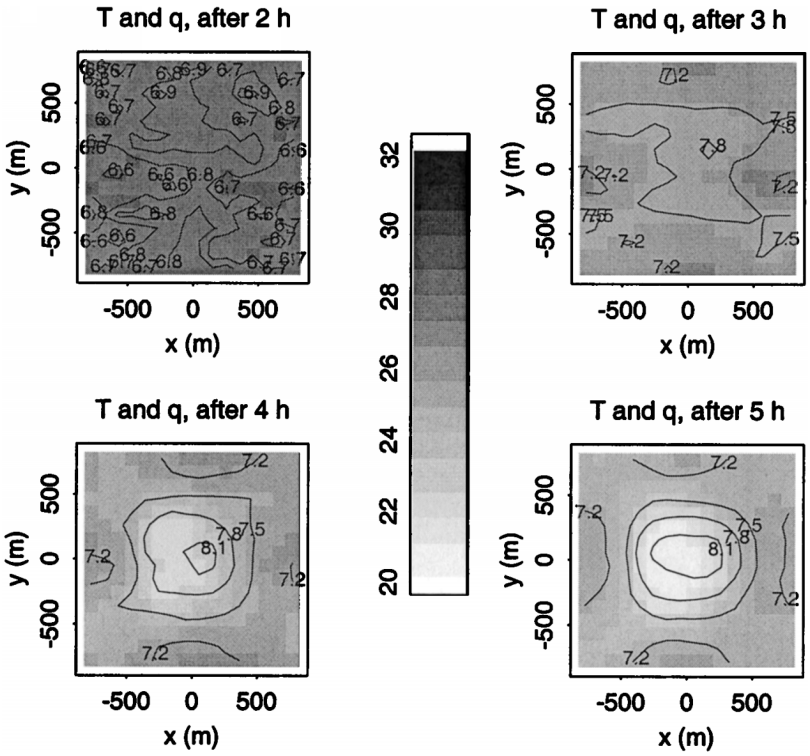

FIG. 17. Contour lines show specific humidity at the surface, for the indicated times. Grayscale is surface temperature in Celsius.

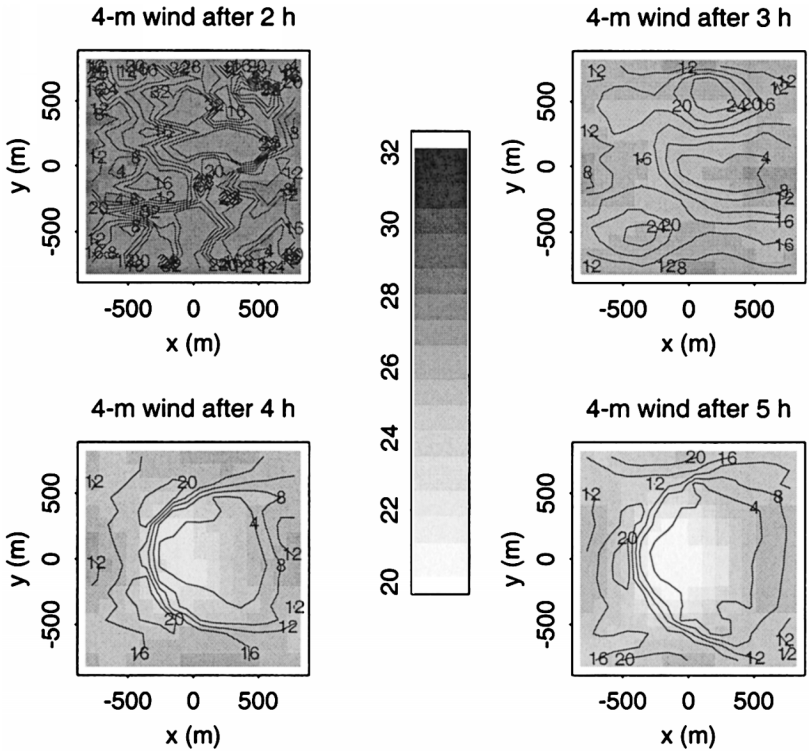

FIG. 18. Contour lines show wind magnitude (cm s^{-1}) at 4 m, for the indicated times. Grayscale is surface temperature in Celsius.

a sharp peak as the term decreases rapidly, remaining close to zero for the last 3 h of the transition, when advection dominates. The effects of advection on the q tendency tend to be negative in higher locations and positive in the valley, pointing to a transport done by the local circulation. This is the reason for the continuous increase in moisture at the higher places, as opposed to the small decrease in the valley.

There are two distinct periods of transition in the simulation, as was observed in the PAM network (Fig. 10). In both the temperature and specific humidity cases, a sharp variation (negative for T, a positive jump for q) happens first, due to the peak in vertical flux divergence. The spatial standard deviation of temperature ($\sigma_{t,\text{spat}}$) starts to increase at the time of the jump, when advection is still not dominant. It suggests that the time of the onset of the transition is not controlled by topography. In the observations, we showed that sheltering played an important role to that matter, with protected stations experiencing earlier wind decay. There are no similar obstructions treated in the LES. For this reason the variation in the time of the onset of the transition is smaller than observed but sufficient to start increasing $\sigma_{t,\text{spat}}$. In a second period, advection distributes the variables around the network. The importance of the first period is more pronounced in the q budgets, in which the peaks in vertical flux divergence are better defined. We suggest that this could be the reason for the more pronounced influence of sheltering in the variation of specific humidity than on temperature (Fig. 10). At sheltered locations, wind decays more rapidly, leading to the early peaks in vertical flux divergence and the consequent q jump and T inflection point. Since the flux divergence peak is sharper in the q budget, this variable would show more influence by sheltering.

Different conclusions regarding q and T can be drawn. The jump in q is responsible for most of its variation during the EET. It means that the early peak in flux divergence is extremely important to the nighttime surface value of q, having important consequences for fog formation and for scalar concentrations in general. Other heterogeneities not included in the simulations such as those induced by obstructions (that cause a sharper jump) would tend to have an important effect on these scalars. Temperature, on the other hand, decreases along the entire EET, as a constant sink of heat exists due to the radiative loss at the surface. Thus, even though the negative peak of vertical flux divergence causes the time of maximum cooling rate (inflection point), it is only a fraction of the total variation this variable experiences along the transition. The topographic dependence of nighttime temperatures is the result from advective processes in the second part of the EET. Other factors that enhance the flux divergence peak, such as sheltering, should affect the temperature as well, but to a lesser degree when compared to the importance that topography has for this variable.

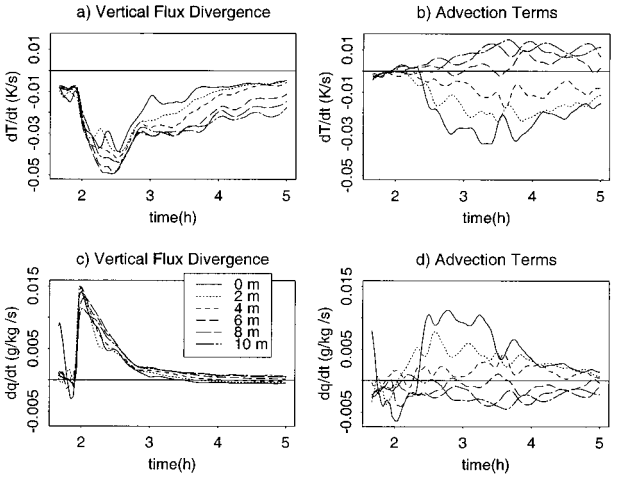

FIG. 19. (a) Vertical flux divergence term in the temperature equation as a function of elevation. The classes are determined in the same way as in Fig. 16. (b) Sum of the three advective contributions for the temperature tendency. (c) Same as in (a) but for the specific humidity tendency. (d) Same as in (b) but for the specific humidity tendency. Legend shown in frame (c) is valid for all frames.

7. Conclusions

1) Enhanced vertical flux divergence at the early evening transition (EET) marks this period as the one with the largest temporal changes in specific humidity and temperature from midafternoon until sunrise. Specific humidity experiences a jump and there is an inflection point in the temperature temporal evolution.
2) Even though temperature decreases throughout the night, the spatial spread in this variable is entirely set during the EET. This was not modeled in the LES, perhaps because different land use and sheltering influences were neglected. We infer that the large spatial variability of the turbulent exchange at EET is a consequence of small eddy size during this period.
3) The transition most frequently occurs under clear skies and light winds. Under these conditions, the q jump occurs nearly at the same time as the inflection point in temperature temporal evolution at most locations. The exceptions are at higher locations, where winds remain high, preventing the decoupling between the surface and the upper boundary layer.
4) Wind decay during EET happens at a faster rate if the wind comes from a direction for which sheltering effects are important. In these cases, larger and earlier specific humidity (q) jumps in moisture are observed. The jumps do not occur at obstructed sites, where wind decays completely and not enough turbulence persists to promote surface fluxes, or at higher stations, that do not experience the transition.
5) The spatial pattern of nocturnal temperature is usually the same from night to night. It depends on topographical features (i.e., the difference between station elevation and the mean elevation in a square area of 3 km $\times$ 3 km surrounding the station), and on land use (urban stations tend to be warmer than rural ones). Large temperature differences occur when only a portion of the stations experiences decoupling. In this circumstance, the decoupled stations are the coldest ones.
6) The Richardson number increases exponentially for a time at EET, with the rate of exponential increase dependent on the rate of TKE decay and, consequently, on obstruction. Places with higher rate of change in Ri are also those with earlier q jumps.
7) Currently used parameterizations of surface exchanges in mesoscale models handle adequately the qualitative aspects of the EET at a single point. However, the high spatial variability observed over an area that is subgrid to these models has serious implications for the accuracy of nighttime forecasts of variables such as minimum temperature or scalar concentration.
8) Large eddy simulations confirm that the q jump and T inflection point are consequences of a peak in vertical flux divergence early in the EET. Advective effects are important at a later stage, when turbulence levels are smaller. Advection distributes the variables around the domain according to topography. In general, vertical flux divergence dominates over advection. However, horizontal advection, strongly dependent on topography, controls the scalar spatial distributions.

Processes that are influenced by surface heterogeneities in general should be subject to the same phenomena described here, making the understanding of their physics at EET essential to the assessment of their spatial distributions. For example, pollutant (such as CO) emissions at urban centers during evening rush hours peak around the time of the transition, likely causing the observation of a very sharp jump in the concentrations. Another example is the CO_2 emission from areas with heterogeneity in soil types and vegetation.

We intend to use the same dataset to assess the effects of nighttime breakdowns of turbulence in the mean variables and their spatial distributions. These intermittent events are similar to the EET processes in the sense that they are very local, causing significant changes in the mean variables, with large variability from place to place. The simulations can be extended to consider other heterogeneities, such as windbreaks, or other types of topography.

Three types of landscape heterogeneity were considered. Topography and land use control the temperature at the end of the EET, with implications in the state of connection between surface and upper boundary layer. Small-scale sheltering affects the rate of wind decay at EET. A model for subgrid variability of temperature and scalars at night could then consist of a simple param-

eterization (e.g., McNider et al. 1995), but allowing for a spectrum of topography, land use, and sheltering fields, typical for a given region. Each surface type could respond in the form of different rates of cooling and wind decay at EET, affecting the state of ''connection.'' The result of such a model would be a spectrum of nighttime temperatures and scalar concentrations for a region, rather than a single value.

Small-scale horizontal variability can have an appreciable effect in large-scale parameterizations of surface–atmosphere exchange. With this purpose, Thornton et al. (1997) developed a method to generate fine resolution maps of variables such as temperature and humidity, accounting for topographical effects. The results presented here can be used to further improve those estimates.

Acknowledgments. O. Acevedo has been supported during graduate studies at The University at Albany, SUNY, by CNPq, the Brazilian Science Foundation.

In the 1980s, initial analysis of the FOG-82 PAM data after the project was completed was done with support from the NSF under Grants ATM8022208 and ATM8317455 and Army Research Office ARO Contract DAAG-29-81-K-0019. G. G. Lala, and the late J. Jiusto, were instrumental in bringing PAM to Albany. G. G. Lala has been a major force for keeping the FOG-82 data available through waves of successive computer systems at ASRC. John Militzer at NCAR worked to assure data quality at the time of the project and has been very supportive since that time.

Completion and extension of this work in the last three years was supported by the NASA TECO program under Project NCC528 and with DOE support from the NE Center at NIGEC, under Project PN0188821449775 as a subcontract from Harvard University.

The work was greatly aided by valuable discussions at NCAR with Piotr Smolarkiewicz, Vanda Grubisic, and Andrzej Wyszogrodzki regarding the use of the model during a 3-week visit by OCA. J. Scolar, of UNESP, Bauru, São Paulo, Brazil, first produced the transmission factor maps (Fig. 3) as a visitor at Albany in 1988.

REFERENCES

Brock, F. V., and P. K. Govind, 1977: Portable automated mesonet in operation. *J. Appl. Meteor.,* **16,** 299–310.

Caughey, S. J., J. C. Wyngaard, and J. C. Kaimal, 1979: Turbulence in the evolving stable boundary layer. *J. Atmos. Sci.,* **36,** 1041–1052.

Derbyshire, S., 1999: Boundary-layer decoupling over cold surfaces as a physical boundary-instability. *Bound.-Layer Meteor.,* **90,** 297–325.

Fitzjarrald, D. R., and G. G. Lala, 1989: Hudson Valley fog environments. *J. Appl. Meteor.,* **28,** 1303–1328.

——, and K. E. Moore, 1994: Growing season boundary layer climate and surface exchanges in a subartic lichen woodland. *J. Geophys. Res.,* **99,** 1899–1917.

Flower, W. D., 1937: An investigation into the variation of the lapse rate of temperature in the atmosphere near the ground at Ismailia, Egypt. Met Office Geophys. Memo. 8, 71, 87 pp.

Fujita, T. T., and R. M. Wakimoto, 1982: Effects of miso- and mesoscale obstructions on PAM winds obtained during Project NIMROD. *J. Appl. Meteor.,* **21,** 840–858.

Geiger, R., 1971: *Climate Near the Ground.* Harvard University Press, 611 pp.

Glendening, J. W., 1996: Lineal eddy features under strong shear conditions. *J. Atmos. Sci.,* **53,** 3430–3449.

Grant, A. L. M., 1997: An observational study of the evening transition boundary-layer. *Quart. J. Roy. Meteor. Soc.,* **123,** 657–677.

Gustavsson, T., M. Karlsson, J. Bogren, and S. Lindqvist, 1998: Development of temperature patterns during clear nights. *J. Appl. Meteor.,* **37,** 559–571.

Harrison, A. A., 1971: A discussion of the temperatures of inland kent with particular reference to night minima in the lowlands. *Meteor. Mag.,* **100,** 97–111.

Haugen, D. A., J. C. Kaimal, and E. F. Bradley, 1971: An experimental study of Reynolds stress and heat flux in the atmospheric surface layer. *Quart. J. Roy. Meteor. Soc.,* **97,** 168–180.

Kaimal, J. C., and J. J. Finnigan, 1994: *Atmospheric Boundary Layer Flows.* Oxford University Press, 289 pp.

LeMone, M. A., and Coauthors, 2000: Land–atmosphere interaction research, early results, and opportunities in the Walnut River watershed in southeast Kansas: CASES and ABLE. *Bull. Amer. Meteor. Soc.,* **81,** 757–779.

Lenschow, D. H., B. B. Stankov, and L. Mahrt, 1979: The rapid morning boundary-layer transition. *J. Atmos. Sci.,* **36,** 2108–2124.

Mahrt, L., 1981: The early evening boundary layer transition. *Quart. J. Roy. Meteor. Soc.,* **107,** 329–343.

——, J. Sun, J. I. MacPherson, R. Dobosy, W. Kustas, and J. Prueger, 1999: Diurnal boundary-layer transitions. *Proc. 13th Symp. on Boundary Layers and Turbulence,* Dallas, TX, Amer. Meteor. Soc., 504–507.

McNider, R. T., D. E. England, M. J. Friedman, and X. Shi, 1995: Predictability of the stable atmospheric boundary layer. *J. Atmos. Sci.,* **52,** 1602–1614.

Meyer, M. B., J. E. Jiusto, and G. G. Lala, 1986: FOG-82: A cooperative field study of radiation fog. *Bull. Amer. Meteor. Soc.,* **67,** 825–832.

Neff, W. D., and C. W. King, 1989: The accumulation and pooling of drainage flows in a large basin. *J. Appl. Meteor.,* **28,** 518–529.

Nieuwstadt, F. T. M., and R. A. Brost, 1986: The decay of convective turbulence. *J. Atmos. Sci.,* **43,** 532–546.

Richardson, L. F., 1920: The supply of energy from and to atmospheric eddies. *Proc. Roy. Soc. London,* **97A,** 354–373.

Smolarkiewicz, P. K., and L. G. Margolin, 1997: On forward in-time differencing for fluids: An Eulerian/semi-Lagrangian non-hydrostatic model for stratified flows. *Atmos.–Ocean,* **35,** 127–152.

Sorbjan, Z., 1996: Numerical study of penetrative and ''Solid Lid'' nonpenetrative convective boundary layers. *J. Atmos. Sci.,* **53,** 101–112.

——, 1997: Decay of convective turbulence revisited. *Bound.-Layer Meteor.,* **82,** 501–515.

Sproken-Smith, R. A., and T. R. Oke, 1999: Scale modelling of nocturnal cooling in urban parks. *Bound.-Layer Meteor.,* **93,** 287–312.

Taylor, G. I., 1917: The formation of fog and mist. *Quart. J. Roy. Meteor. Soc.,* **43,** 241–268.

Tennekes, H., and J. L. Lumley, 1972: *A First Course in Turbulence.* The MIT Press, 300 pp.

Thornton, P. E., S. W. Running, and M. A. White, 1997: Generating surfaces of daily meteorological variables over large regions of complex terrain. *J. Hydrol.,* **190,** 214–251.